

Three-dimensional tomography using a cubic-phase plate extended depth-of-field system

Daniel L. Marks, Ronald A. Stack, and David J. Brady

Department of Electrical and Computer Engineering, Beckman Institute, University of Illinois at Urbana-Champaign, Urbana, Illinois 61801

Joseph van der Gracht

Army Research Laboratory, AMSRL-SE-EO, 2800 Powder Mill Road, Adelphi, Maryland, 20783

Received July 30, 1998

We use cubic-phase plate imaging to demonstrate an order-of-magnitude improvement in the transverse resolution of three-dimensional objects reconstructed by extended depth-of-field tomography. Our algorithm compensates for the range shear of the cubic-phase approach and uses camera rotation to center the reconstructed volume on a target object point. © 1999 Optical Society of America

OCIS codes: 110.6880, 110.6960, 110.4850, 220.1230, 100.1830.

Inversion of the line integrals associated with extended depth-of-field (EDF) imaging has been used in the x-ray regime to reconstruct three-dimensional (3D) objects.¹⁻³ Related ray-projection techniques have been used in the visible range to reconstruct radiant sources.⁴ In Ref. 5 we used EDF pinhole imaging to reconstruct a 3D volume in the visible spectral range. The relatively poor transverse resolution of the pinhole camera is a shortcoming for this technique. The cubic-phase plate (CPP) EDF system⁶⁻⁹ measures similar line integrals while maintaining a relatively large system aperture. The larger aperture yields superior transverse resolution and light-gathering efficiency. In this Letter we describe the use of a CPP EDF system to form 3D images.

Aperture modulation in CPP imaging yields a point spread function (PSF) that is relatively insensitive to defocus. Digital deconvolution of the PSF yields an image focused at all depths for which the range invariance holds. The transmittance of a CPP is $t(x, y) = \exp[j\alpha(x^3 + y^3)]$.⁶ Assuming an unbounded aperture is the Airy Ai function, and γ is the defocus parameter ($1/z + 1/z' - 1/f$), the PSF for quasi-monochromatic imaging between a source point at (x, y, z) and an image point at (x', y', z') can be shown to be

$$\begin{aligned} \text{PSF}\left(x' + \frac{z'}{z}x, y' + \frac{z'}{z}y, z, z'\right) &= \frac{1}{\alpha^{4/3}} Ai^2\left\{-\frac{\alpha^{2/3}}{3^{1/3}}\left[\frac{2\pi}{\lambda z'\alpha}\left(x' + \frac{z'}{z}x\right) + \frac{\pi^2\gamma^2}{3\alpha^2\lambda^2}\right]\right\} \\ &\times Ai^2\left\{-\frac{\alpha^{2/3}}{3^{1/3}}\left[\frac{2\pi}{\lambda z'\alpha}\left(y' + \frac{z'}{z}y\right) + \frac{\pi^2\gamma^2}{3\alpha^2\lambda^2}\right]\right\}, \quad (1) \end{aligned}$$

where $Ai(x)$ is the Airy Ai function¹⁰ and f is the focal length. To form a range-independent deblurred image, we deconvolve the PSF from the detected image. The deblurred image is sheared with respect to range, but the shear can be removed in 3D imaging. In practice, the finite plate aperture limits the range independence of the PSF. The in-

finite aperture approximation assumes that the cubic phase varies more rapidly than the natural quadratic phase at the aperture edge. This criterion implies that γ must be comparable with $\alpha d\lambda$, where d is the system aperture.

We consider the CPP EDF camera imaging source volume in Fig. 1. The camera acquires a series of images as it is translated laterally to the optical axis. The lateral position of the center of the camera principal plane is denoted \hat{x} . Unlike in Ref. 5, the camera axis rotates about a point in the source space during lateral displacement. The rotation centers the reconstructed range field on the pivot point. The nominal distance from the pivot point to the center of the camera aperture is z_0 . We form 3D images by capturing a series of distorted 2D images for various values of \hat{x} , digitally deconvolving each frame to obtain an in-focus EDF 2D image and transforming the series of EDF images to obtain a 3D source model.

Assuming that the pivot point satisfies the imaging condition, $z_0 = z'f/z' - f$, and defining $\Delta z = z - z_0$, the origin of the PSF in the (x', y') plane for the source point at (x, y, z) is

$$\begin{aligned} \frac{x'}{z'} &= -\frac{x}{z} - \frac{\pi}{6\alpha\lambda z_0^2}\left(\frac{\Delta z}{z}\right)^2, \\ \frac{y'}{z'} &= -\frac{y}{z} - \frac{\pi}{6\alpha\lambda z_0^2}\left(\frac{\Delta z}{z}\right)^2. \end{aligned}$$

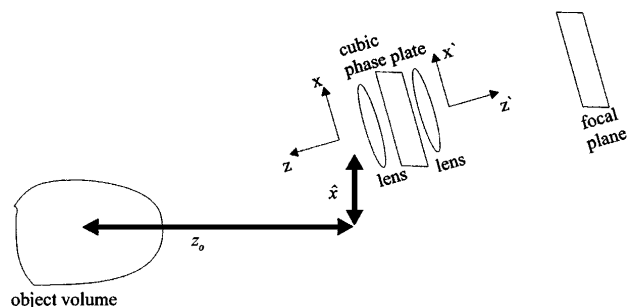


Fig. 1. System geometry.

For a given value of \hat{x} the deconvolved image is approximated by

$$\begin{aligned}
 I(\xi, \eta) = & \int P(x, y, z) \delta \left[\frac{\xi}{z'} + \frac{(x + \hat{x})z_0}{z} - \frac{\hat{x}}{z_0} \right. \\
 & + \left. \frac{\pi}{6\alpha\lambda z_0^2} \left(1 - \frac{z_0}{z}\right)^2 \right] \delta \left[\frac{\eta}{z'} + \frac{y}{z} \right. \\
 & + \left. \frac{\pi}{6\alpha\lambda z_0^2} \left(1 - \frac{z_0}{z}\right)^2 \right] dx dy dz, \quad (2)
 \end{aligned}$$

where $P(x, y, z)$ is the source power density. Inverting Eq. (2) as in Ref. 5, we Fourier transform with respect to (ξ, η) and introduce the variables $x_p = (z'/z)x$, $y_p = (z'/z)y$, $q = k_\xi z' \hat{x}$, and $z_p = 1/z$ to obtain

$$\begin{aligned}
 \tilde{I}(k_\xi, k_\eta, q) = & \int P(x_p, y_p, z_p) \exp(jk_\xi x_p) \exp(jk_\eta y_p) \\
 & \times \exp(jqz_p) \exp(-jqz_{0p}) \exp \left[jk_\xi \frac{\pi z'}{6\alpha\lambda z_0^2} \right. \\
 & \times \left. (1 - z_0 z_p)^2 \right] \exp \left[jk_\eta \frac{\pi z'}{6\alpha\lambda z_0^2} \right. \\
 & \times \left. (1 - z_0 z_p)^2 \right] dx_p dy_p dz_p. \quad (3)
 \end{aligned}$$

Fourier inversion of Eq. (3) yields the focused 3D source distribution evaluated at

$$\begin{aligned}
 \left[x_p + \frac{\pi z'}{6\alpha\lambda z_0^2} (1 - z_0 z_p)^2, \right. \\
 \left. y_p + \frac{\pi z'}{6\alpha\lambda z_0^2} (1 - z_0 z_p)^2, z_p - \frac{1}{z_0} \right],
 \end{aligned}$$

where (x_p, y_p, z_p) are the Fourier conjugate variables for (k_ξ, k_η, q) . The range in (k_ξ, k_η, q) over which $\tilde{I}(k_\xi, k_\eta, q)$ can be sampled defines the 3D bandpass, or band volume, for the imaging system. The 3D Fourier transform of the band volume is the system impulse response. Since the longitudinal Fourier sampling coordinate, q , is proportional to the transverse sampling coordinate, k_ξ , there is a missing cone in the band volume.¹¹ The longitudinal resolution for low-transverse-frequency objects is limited as a result of the missing cone.

We confirmed our model for 3D imaging by experimentally measuring the impulse response. Our experimental system consisted of two 20-cm focal-length lenses (yielding a nearly 10-cm effective focal length) separated by a 1.2-cm-aperture CPP pupil with $\alpha = 58.6 \text{ cm}^{-3}$. We placed the sources and the focal-plane array approximately 20-cm from the CPP to achieve nominal 1:1 imaging. The focal-plane array was a 512 by 512, 1.27-cm-square Princeton Instruments back-illuminated 16-bit-resolution CCD camera. The camera and the imaging system were attached to metal rods and placed on a computer-controlled Newport rotation stage, which was attached to an Aerotech computer-controlled translation stage with 5-cm travel.

A 660-nm laser diode that operated as a LED served as the point source for building the digital deconvolution filter.

We placed the source 20 cm from the cubic-phase mask and sensed the raw PSF at the focal plane. Because the cubic-phase transmittance is rectangularly separable, we sampled the PSF on the x and y axes and computed an inverse weighted Wiener filter of the sampled data to obtain separate vertical and horizontal deconvolution filters. We selected the filter weight to band limit the inverse filter to prevent noise from dominating the image. We used $\sim 50\%$ of the bandwidth of the system. The digitally deconvolved PSF occupied from 1.5 to 2 camera pixels, and the raw PSF covered approximately 15 pixels. The CCD camera's pixels were $22 \mu\text{m}$ square.

We acquired frames by translating the imaging system at fixed intervals. At each acquisition position we rotated the camera toward the source pivot point and integrated the intensity on the focal plane for 30 ms. The total length of travel of the translation stage was 4.5 cm, and the total rotation angle was $\sim 13^\circ$. 256 images were taken over this path. The projections were sampled at 512 by 512 pixels and deconvolved. After deconvolution, we resampled the projections to compensate for the camera rotation and to compress the frame size to 256 by 256. The resampled images corresponded to projections displaced linearly in the tangents of the angles as measured from each projection origin. We combined the projections into a 3D model of the source by computing the 2D Fourier transform of each image, resampling the k_ξ axis onto a Cartesian grid, and then taking the 3D Fourier transform. These operations were performed in $O(N^3 \log N)$ time.

We tested our system by reconstructing the 660-nm point source at approximate distances of 15, 17, 20, and 25 cm from the principal plane of the imaging system. Figure 2 shows transverse slices through each of the reconstructed 3D PSF's. The axes correspond to projection angle. Each axis spans 52 mrad. The 15-cm image is significantly worse because the sharp increase in defocus as one approaches the principal plane causes the invariant raw PSF approximation to fail. Longitudinal slices through the reconstructed 3D PSF's are shown in Fig. 3. The horizontal axis

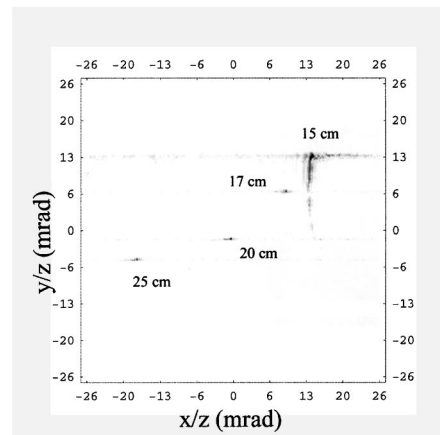


Fig. 2. Superimposed lateral cross sections of four digitally reconstructed 3D PSF's, labeled with their distances from the principal plane. The axes are angles labeled in milliradians.

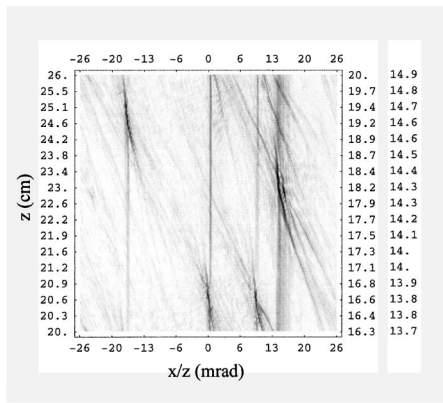


Fig. 3. Superimposed longitudinal cross sections of four digitally reconstructed 3D PSF's labeled with their distances from the principal plane. The horizontal axis is angle labeled in milliradians, and the vertical axis is projective depth labeled in centimeters. The vertical scale is plotted linearly in $1/z$ space but is marked in z space.

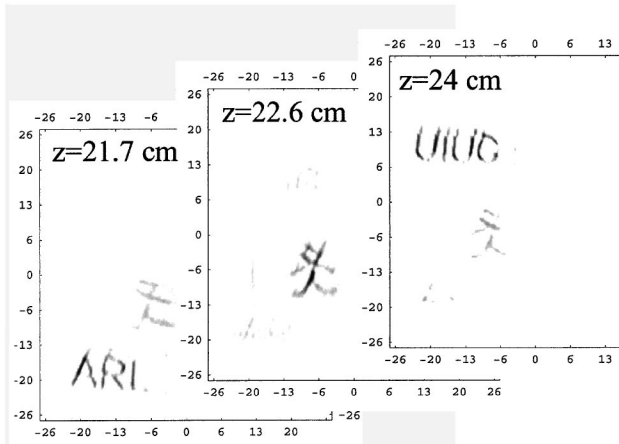


Fig. 4. Three lateral slices through the reconstruction of a demonstration source. The axes correspond to angular position relative to the principal axis in milliradians.

represents the transverse resolution in milliradians, and the vertical axis represents the projective depth in inverse meters. The vertical axis spans 1.16 m^{-1} . The projective depth is the depth that is linear in z^{-1} and not in z . The vertical axes are marked in z coordinates, however. Three separate axes are shown because the reconstructed sources are aliased onto the plot from three separate reconstruction patches. The reconstruction uses a projective depth step size of 0.0045 m^{-1} , which is determined by the total linear length of travel of the camera ($\hat{x}_{\text{span}} = 4.5 \text{ cm}$) and the angular resolution of the camera ($\theta_{\text{res}} = 0.2 \text{ mrad}$) by $z_{\text{res}}' = \theta_{\text{res}}/\hat{x}_{\text{span}}$. The achieved resolution is limited by incomplete coverage of the 3D Fourier space and the band limit in the deconvolution kernel. The measured longitudinal sizes of the source are 0.216 m^{-1} (4.9 mm) for the 15-cm trial, 0.153 m^{-1} (4.4 mm) for the 17-cm trial, 0.122 m^{-1} (4.8 mm) for the 20-cm trial, and 0.189 m^{-1} (11.8 mm) for the 25-cm trial. As indicated by the 17- and the 25-cm reconstructions, the depth-of-field exceeds 1 m^{-1} . This range is consistent with the value of $\alpha d \lambda = 0.46 \text{ m}^{-1}$

for our system. The pinhole size needed to achieve this depth of field at 660 nm is $800 \mu\text{m}$. The transverse resolution for the pinhole system would be approximately one order of magnitude worse than the 80–100- μm resolution indicated for the cubic-phase system in Fig. 2.

Figure 4 demonstrates 3D reconstruction of a complex source. The source consisted of white-on-black text and images on small strips of paper. The papers were illuminated by two broadband fluorescent lamps to provide uniform illumination. The paper in the front had the letters ARL on it, the paper in the middle had a stick figure likeness of a man, and the paper in the rear had the letters UIUC on it. The exposed sections of the papers were approximately 0.3 by 0.4 cm in size. Figure 4 shows three cross sections of the source at various depths. The intensity of the source is shown in reverse, and the negative intensity artifacts that are due to the PSF have been filtered out. Although the reconstruction is fairly accurate on these planes, it should be noted that the PSF spreads the images over many planes, as can be seen because the stick figure man in the center plane appears weakly in the other two planes.

The cubic-phase plate extended depth-of-field system yields substantially better transverse resolution than a pinhole with comparable depth of field. Since the transverse resolution is coupled to longitudinal resolution through the q variable, increased transverse resolution translates directly into improved longitudinal resolution for a given scan range. Further investigation into the optimality of the cubic-phase modulation, the effect of noise in deconvolution, and deconvolution filter design is required for characterization and exploitation of this improvement in longitudinal resolution.

This work was supported by the Defense Advanced Research Projects Agency through ARO grant 38310-PH. D. Marks acknowledges the support of a National Science Foundation Graduate Fellowships.

References

1. Y. W. Chen, N. Miyanaga, and N. Yamanaka, *J. Appl. Phys.* **68**, 1483 (1990).
2. J. W. V. Gissen, M. A. Viergever, and C. Graaf, *IEEE Trans. Med. Imaging* **MI-4**, 91 (1985).
3. L. I. Yin and S. M. Seltzer, *Appl. Opt.* **32**, 3726 (1993).
4. I. Ashdown, *J. Illum. Eng. Soc.* **22**, 163 (1993).
5. D. Marks and D. Brady, *Opt. Lett.* **23**, 820 (1998).
6. E. Dowski and W. Cathey, *Appl. Opt.* **34**, 1859 (1995).
7. J. van der Gracht, E. Dowski, and W. Cathey, *Proc. SPIE* **2537**, 279 (1995).
8. J. van der Gracht, E. Dowski, M. G. Taylor, and D. M. Deaver, *Opt. Lett.* **21**, 919 (1996).
9. S. Bradburn, W. Cathey, and E. Dowski, *Appl. Opt.* **36**, 9157 (1997).
10. W. F. Magnus, F. Oberhettinger, and R. Soni, *Formulas and Theorems for the Special Functions of Mathematical Physics* (Springer-Verlag, New York, 1966), p. 76.
11. M. Y. Chiu, H. H. Barrett, R. G. Simpson, C. Chou, J. W. Ardent, and G. R. Gindi, *J. Opt. Soc. Am.* **69**, 1323 (1979).